Line-Scanning Microphotolysis for Diffraction-Limited Measurements of Lateral Diffusion

Peter Wedekind, Ulrich Kubitscheck, Oliver Heinrich, and Reiner Peters
Institut für Medizinische Physik und Biophysik, Westfälische Wilhelms-Universität, 48149 Münster, Germany

ABSTRACT Fluorescence microphotolysis was combined with confocal laser-scanning microscopy to yield a method, herein referred to as line-scanning microphotolysis (LINESCAMP), for the measurement of molecular transport at a lateral resolution of ~0.34 μm and a temporal resolution of ~0.5 ms. A confocal microscope was operated in the line scan mode, while the laser beam power could be switched during scanning between low monitoring and high photolysing levels in less then a microsecond. The number and location of line segments to be photolysed could be freely determined. The length of the photolysed segments could be also chosen and was only limited by diffraction. Together with instrumentation a new, completely general, theoretical framework for the evaluation of diffusion measurements was developed. Based on the numerical simulation of diffusion processes employing a modified Crank-Nicholson scheme, the theory could be applied to any photobleaching geometry and profile as the initial condition and took into account the convolution with the microscope point spread function. With small diffraction-limited areas, the method yielded accurate values for diffusion coefficients in the range between approximately 10^{-4} and 1 $\mu m^2 s^{-1}$. A first application of the method to the diffusion of a fluorescently labeled tracer inside the cell nucleus showed the potential of the method for the study of complex biological systems.

INTRODUCTION

Spatially resolved measurements of lateral transport can provide important clues to the functional architecture of biological systems. For instance, based on lateral mobility measurements by photobleaching (Edidin et al., 1992b) and single particle tracking (Kusumi et al., 1993), the plasma membrane is now believed to consist of domains that are 0.3–0.6 μm wide (for a review, see Edidin, 1992a). Lateral diffusion measurements also suggested that the cytosol contains a network of entangled filaments (for a review, see Luby-Phelbs, 1994). The cell nucleus is thought to harbor an intricate system of chromosome domains and interchromatin channels (Manuelidis, 1985; Schardin et al., 1985; Pinkel et al., 1988; De Boni, 1994; Blobel, 1985; Spector, 1990; Cremer et al., 1993; Zachar et al., 1993), an important hypothesis that could be tested by high-resolution measurements of lateral mobility.

For these and other reasons great efforts are currently being undertaken to develop methods by which lateral molecular transport can be analyzed at high spatial resolution. Single particle tracking (Barak and Webb, 1981; De Brabander et al., 1985; Anderson et al., 1992) and scanning optical near-field microscopy (Pohl et al., 1984; Lewis et al., 1984; Betzig et al., 1991) are novel, particularly promising approaches to that goal. On the other hand, fluorescence correlation spectroscopy (Elson and Magde, 1974; Magde et al., 1974) and fluorescence photobleaching methods (Peters et al., 1974; Edidin et al., 1976; Jacobson et al., 1976; Axelrod et al., 1976) have been in use for many years. In particular, photobleaching methods have amply proved their usefulness in biological studies (for review, see Peters, 1981; Peters and Scholz, 1991; Edidin, 1992b; Ishihara and Jacobson, 1993).

In the conventional fluorescence photobleaching method, a stationary laser beam is directed into the vertical illuminator of a fluorescence microscope and focused into the sample to yield an irradiated area, usually of ~1 μm radius. In the irradiated area fluorescence is irreversibly photobleached by a light pulse of approximately 1 mW power and 0.1 s duration. After photolysis the laser beam power is largely reduced to monitor the dissipation of the fluorescence inhomogeneity by lateral transport. The spatial resolution of conventional fluorescence photobleaching experiments could be increased to approximately 0.3 μm by focusing the laser beam down to the diffraction limit. This, however, would require additional measures, such as an extraordinary mechanical stability, a high temporal resolution of fluorescence measurements, and a largely increased efficiency of photobleaching. Most of these problems can be overcome by beam scanning, as first shown by Koppel (1979). He constructed a photobleaching apparatus in which the irradiated area could be sequentially positioned at 12 locations on the x coordinate. The availability of commercial confocal laser scanning microscopes (CLSM) opened new possibilities for photobleaching methods (Scholz et al., 1988). Thus, Blonk et al. (1993) employed the line-scanning mode of a CLSM, as we have in the present study, but using the CLSM essentially in its commercial form, obtained only a small spatial (radius of photobleached area ~4 μm) and a moderate temporal (photolysis time ~70 ms) resolution.

Recently we introduced (Wedekind et al., 1994) a new photobleaching method, intending to make full use of the advantages of the CLSM. The method, referred to as scanning microphotolysis (SCAMP), can be easily installed on

Received for publication 26 February 1996 and in final form 17 May 1996.
Address reprint requests to Dr. Reiner Peters, Institut für Medizinische Physik und Biophysik, Robert-Koch-Strasse 31, 48149 Münster, Germany. Tel.: 49-251-836933; Fax: 49-251-835121; E-mail: petersr@uni-muenster.de.

0006-3495/96/09/1621/12 $2.00

any CLSM and has a broad range of applications. A CLSM was complemented with a fast programmable optical switch, the SCAMPER, permitting us to turn the laser beam on and off during scanning according to a freely programmable image mask. Thus, within the scanned field areas of virtually any size, geometry, and number can be selected for photolysis, and the dissipation of the photolysis pattern can be monitored by repetitive imaging at full confocal resolution (Wedekind et al., 1994; Kubitscheck et al., 1994; Schmidt et al., 1994; Tschödrich-Rotter et al., 1996). Moreover, combined with two-photon absorption (Kubitscheck et al., 1996), SCAMP achieves a true three-dimensional selectivity of photolysis.

Although SCAMP features the high spatial resolution inherent in confocal imaging, its temporal resolution is limited by the image repetition time of the CLSM, typically 0.1–1.0 s. In the present study a new high-resolution version of SCAMP, referred to as LINESCAMP, was developed. By reconstructing the SCAMPER, using a CLSM of latest design and, most importantly, employing the line scan mode of the CLSM, the time resolution could be increased to ~0.5 ms. The spatial resolution was only limited by diffraction (~0.34 μm). Concomitantly with the experimental methods, a new theoretical framework was developed for evaluating measurements of two-dimensional lateral diffusion. The theory is based on the numerical iteration of the diffusion equation, can be applied to arbitrary photolysis geometries, and takes the convolution of scanned beam and photolysis pattern into account. Furthermore, it has the potential to be extended to photobleaching measurements of three-dimensional diffusion. The new experimental and theoretical methods for lateral diffusion measurements were carefully characterized by using simple test samples. Preliminary measurements on cell nuclei demonstrated the potential of LINESCAMP for the analysis of heterogeneous biological systems.

PRINCIPLE OF LINE SCANNING MICROPHOTOLYSIS

In LINESCAMP experiments a modified CLSM is employed to obtain a confocal x,y scan of a specimen. The image is used to select a line and to mark on this line segments to be photolysed. The length and position of the segments as well as their number are freely selectable. Switching to the line scan mode, the laser beam is repetitively scanned at high speed along the selected line. Fluorescence originating from the focal volume is measured during scanning pixel by pixel, and the digitalized intensity values are continuously written into the memory. Thus, displaying the memory on a video screen produces an "image" whose horizontal (x) coordinate represents the position of the beam along the scanned line, and whose vertical (y) coordinate represents time. A high time resolution results from the circumstance that the time per line is small, e.g., ~0.5 ms, in the CLSM used in this study. The further procedure is illustrated in Fig. 1. Among line scans one may discriminate between imaging and bleaching ones. The experiment starts with a few imaging line scans (Fig. 1, *A* and *B*) at low, nonbleaching beam power. Then a single or a few bleaching line scans (Fig. 1, *C–F*) follow at a greatly increased beam power. However, the laser beam is not continuously switched on during these bleaching scans, but only when inside previously selected sections of the scanned line (Fig. 1, *D* and *E*). After photolysis the laser beam power is reduced to the initial low level (Fig. 1 *F*), and the memory is filled with imaging line scans to monitor the dissipation of the bleaching pattern (Fig. 1, *G* and *H*). Definition of the sections to be bleached (Fig. 1, *D* and *E*) as well as the rapid switching between laser beam powers are accomplished by a special device, the SCAMPER, described below.

THEORETICAL FRAMEWORK FOR TWO-DIMENSIONAL DIFFUSION MEASUREMENTS BY LINE-SCANNING MICROPHOTOLYSIS

The outlined procedure differs from that of conventional photobleaching experiments in that a scanned instead of a stationary laser beam is used to induce photolysis and to monitor the time development of the photolysis pattern, and in that the photolysed area in general is not radially symmetrical. Thus, the theoretical approach used to analyze

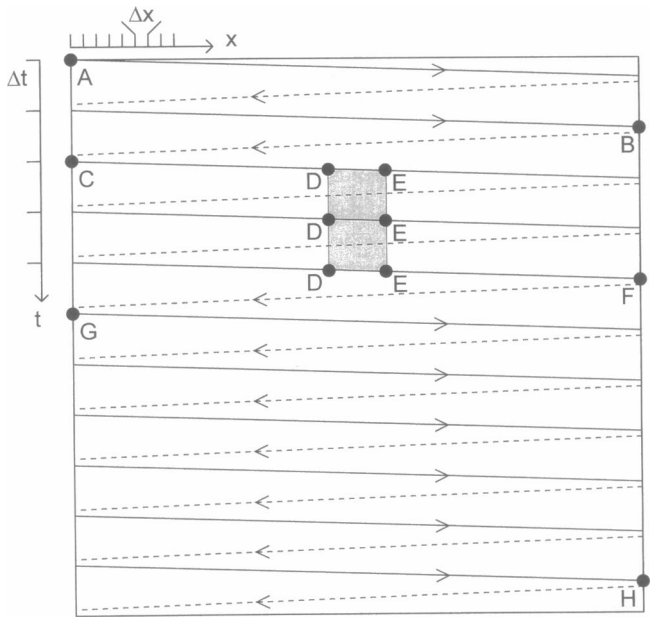

FIGURE 1 Principle of line-scanning microphotolysis. A confocal microscope is operated in the line scan mode, in which a laser beam is scanned along a single line in the x direction. The fluorescence intensities of the pixels are written line by line into the video memory to yield an "image," the coordinates of which are length (horizontal) and time (vertical). The laser beam power can be switched during scanning between low imaging levels (A-B, G-H) and high photolysing levels (D-E). The number and position of line segments to be photolysed can be freely determined. The size of the photolysed segments is limited only by diffraction.

conventional photobleaching measurements of two-dimensional lateral mobility (Axelrod et al., 1976; Soumpasis, 1983) does not apply to the present case. We therefore developed a new versatile numerical approach that is applicable to any photolysis geometry and that takes into account the convolution of monitoring beam and photolysis pattern.

In analogy to conventional photobleaching experiments, we considered an idealized specimen consisting of an infinite plane. Before photolysis fluorescent molecules were thought to be uniformly distributed in the plane and to comprise two populations, a mobile fraction, f_{mob}, with lateral diffusion coefficient D, and an immobile fraction, $f_{immob} = 1 - f_{mob}$, with $D \approx 0$. Photolysis was assumed to occur at the origin of the coordinate system at time $t = 0$, and to be instantaneous, i.e., the time T required for photolysis was assumed to be negligibly small compared to diffusion times. Photobleaching was assumed to be irreversible, and of first order with rate constant $\alpha I_{in}(x,y)$, where $I_{in}(x,y)$ denotes the total light intensity deposited in the sample during repeated bleaching scans.

The special conditions prevailing in LINESCAMP experiments were accounted for as follows. Scanning was assumed to proceed along the x axis. The illumination pattern of a laser beam focused down to the diffraction limit is theoretically given by a radialy symmetrical Airy pattern (Born and Wolf, 1986). Experimentally we found, however, that the intensity distribution could be well approximated by a radially symmetrical Gaussian function with a standard deviation σ_{NA} depending on the numerical aperture (NA) of the microscope objective lens. During the time that the scanning beam irradiated the sample at bleaching intensity, it advanced by a (Fig. 1, D and E), thus giving rise to an elongated, elliptical intensity profile:

$$I_{in}(x, y) = \int_{-a/2}^{+a/2} A_{in} e^{-[(x-x')^2+y^2]/2\sigma_{NA}^2}\, dx'. \qquad (1)$$

Here A_{in} designates the line density of the illumination intensity. Using this expression, the distribution of bleached fluorophores immediately after photolysis ($t = 0$) was

$$c(x, y, 0) = c_0(1 - e^{-\alpha T I_{in}(x,y)}), \qquad (2)$$

where c_0 is the spatially constant fluorophore density before photolysis. After photolysis the total concentration of bleached fluorophores, $c(x,y,t)$, was the sum of that of the mobile fraction, $c_m(x,y,t)$, and that of the immobile fraction, $c_{im}(x,y)$. Whereas $c_{im}(x,y)$ would not change with time, $c_m(x,y,t)$ was governed by the diffusion equation

$$\frac{\partial c_m(x, y, t)}{\partial t} = D\left[\frac{\partial^2}{\partial x^2} + \frac{\partial^2}{\partial y^2}\right] c_m(x, y, t), \qquad (3)$$

with the boundary condition $c_m(x,y\to\infty,t) = 0$. D denoted the diffusion coefficient. Equation 3 was numerically solved under the given boundary condition and the initial condition, Eqs. 1 and 2, employing the modified two-dimensional Crank-Nicholson iteration scheme outlined in the Appendix.

To take a measurement, a laser beam of greatly attenuated power was scanned along the x axis, and the space- and time-dependent fluorescence was registered via a confocal pinhole by a photomultiplier. Thus, imaging of the bleaching pattern was basically determined by the confocal microscope point spread function, $PSF(x,y)$. However, because the monitoring beam was quickly scanned across the photolysed area along the x coordinate, the x-t image actually represented a convolution of $c(x,y,t)$ and $PSF(x,y)$ according to

$$F(x, y = 0, t) = k \int_{-\infty}^{+\infty} \int_{-\infty}^{+\infty} PSF(x', y') \times [c_0 - c_m(x - x', -y', t) - c_{im}(x - x', -y')]\, dx'\, dy'. \qquad (4)$$

The factor k is an overall constant taking quantum efficiency, excitation, and detection probabilities into account.

Experimental data were evaluated in terms of D and f_{mob} by a computer program performing the following tasks:

1. The pixel values belonging to the photolysed section of a scanned line (Fig. 1, D and E) were averaged. This yielded a fluorescence recovery curve, i.e., the time dependence of the average intensity of the photolysed area. When several sections of a line were photolysed (cf. Fig. 5), each of the sections was averaged independently to yield a set of fluorescence recovery curves, as shown, for instance, in Fig. 6.

2. The concentration distribution immediately after photolysis was simulated using Eqs. 1 and 2. In the data analysis program the integral in Eq. 1 was replaced by summation over $n = a/\Delta x$ Gaussians, where Δx was the pixel size. Each of the Gaussians was centered on a different pixel along the line segment of length a. The result of this summation was used in Eq. 2 for the calculation of the initial condition. Here the factor αT determined the depth and shape of the photobleaching profile.

3. The time evolution of the initial concentration distribution was calculated by the modified Crank-Nicholson scheme in the Appendix. The size of the discretization steps Δx and Δy used in the numerical integration was set according to the pixel size, and Δt was chosen in accordance with the line repetition time, i.e., 4.55 ms, 2.22 ms, 1.05 ms, or 0.525 ms, depending on the scanning mode selected (see below).

4. The convolution of the time-dependent concentration distribution with the microscope point spread function was calculated according to Eq. 4. Again the integration was replaced by the appropriate matrix multiplication. The intensity values of the $n = a/\Delta x$ pixels of the photolysed line segment were averaged and presented a single time-dependent recovery signal.

5. Eventually, the simulated recovery curve was fitted to the experimental by minimizing the χ^2 function of the experimental and simulated data using a Simplex algorithm

(Press et al., 1992). Variables were the extent of bleaching αT, the length of the bleached line segment a, the diffusion constant D, and the mobile fraction f_{mob}.

MATERIALS AND METHODS

Specimen for determination of photobleaching parameters and diffusion measurements

For the visualization of photobleaching patterns gel layers containing immobilized fluorescein were generated. A 70-kDa dextran labeled with fluorescein isothiocyanate (FITC-dextran) was added to a solution of acrylamide (final concentration 35% by weight), ammonium persulfate, and *N,N,N′,N′*-tetramethylethylendiamide. A small volume of the mixture was deposited on a glass slide and covered with a coverslip. By variation of the volume (2–10 μl) and the pressure applied to the coverslip during polymerization, layers ranging in thickness between 2 and 50 μm were generated.

For measurements of lateral diffusion, b-phycoerythrin (Molecular Probes, Eugene, OR) was dissolved in a glycerol/water mixture (89.85/11.15, w/w). This was spread as a very thin layer between a slide and a coverslip. In addition, FITC-dextrans of various average molecular weights (40, 70, 150, or 2000 kDa; obtained from Sigma, Deisenhofen, Germany) were dissolved in 1 M Tris buffer (pH 8.8) at a final concentration of 5–10 mg/ml. These stock solutions were mixed with glycerine (40–90%, w/v). To yield perfectly homogeneous mixtures, the solution was heated to 70°C for 24 h. The solutions (1–5 μl) were placed on glass slides, covered with coverslips, and compressed for several hours. Afterward, samples were allowed to relax for 24 h to minimize internal flow. The procedure yielded homogeneously fluorescent layers of 1.5–5 μm thickness.

Cells and their preparation for intranuclear diffusion measurements

3T3 cells were cultured in Dulbecco's minimum essential complete medium (Boehringer-Mannheim) at 37°C, 5% CO_2, and passaged every 3 days. For labeling, cells were used 24–48 h after seeding on coverslips. Cells on coverslips were washed and permeabilized with Triton X-100 (Merck, Darmstadt, Germany; 50 μg/ml) for 6–8 min at 4°C. After washing, coverslips were mounted upside down on glass slides, using tape spacers to create small chambers that were filled with 5 μl dye solution (FITC-dextran in Tris buffer; 2 mg/ml). Samples were allowed to equilibrate for 20 min after mounting before microscope analysis.

LINESCAMP instrumentation

The set-up used in the present study is shown schematically in Fig. 2. It consisted of a 2-W argon ion laser (model 164/265; Spectra Physics, Darmstadt, Germany), a fast and programmable optical switch, the SCAMPER, and a CLSM (model TCS; Leica, Heidelberg, Germany). The laser was usually operated at 488 nm and 300 mW. The laser beam was directed into the SCAMPER, passing there a beam deviation/photoshutter assembly and an acoustooptical modulator (AOM) (model TEM 80–2; Bimrose, Champbell, Baltimore, MD). The AOM-generated first diffraction order was guided onto the input aperture of the CLSM via fiber optics.

The SCAMPER, a profoundly improved version of the one described previously (Wedekind et al., 1994), could be operated in either of two modes, depending on the required time resolution and contrast ratio. In the first mode the photoshutter was permanently opened and the AOM driver was operated in the analog mode, using a computer-controlled interface to set the control voltage of the AOM driver to 0.0, 0.005, or 5.0 V, respectively. This yielded laser beam powers in the object of approximately <100 nW ("zero" level), 1 μW (imaging level), and 1 mW (photolysis level), respectively. The time required for switching between power levels amounted to a few nanoseconds. The maximum contrast between imaging and photolysis levels was 2000:1. Although this was sufficient for all experiments described in this paper, there might be situations where even higher contrast ratios are required. In such cases the SCAMPER could be operated in the second mode. The AOM was operated in the digital mode to rapidly switch the beam power between zero and the photolysis levels. However, switching between imaging and photobleaching power levels was achieved by the beam deviation/photoshutter assembly indicated in Fig. 2. In this assembly the contrast between imaging and photobleaching light levels was adjusted by neutral density filters and hence could be chosen at will. The switching time was limited by the opening and closing times of the photoshutter, i.e., about 1 ms.

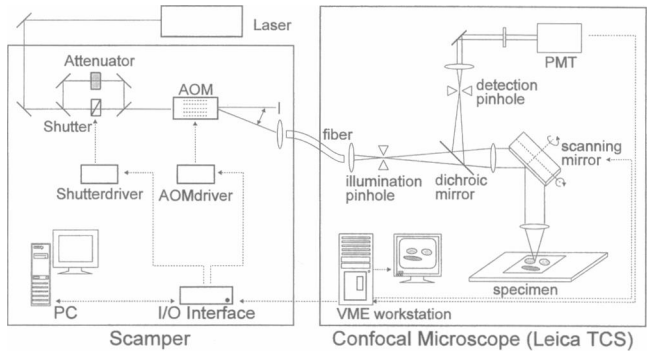

FIGURE 2 Schematic view of the instrument used for line-scanning microphotolysis. A confocal laser scanning microscope was combined with a powerful laser and a fast beam switch, referred to as SCAMPER. The SCAMPER essentially consists of an acoustooptical modulator, a beam deviation, and a computer.

The CLSM could be operated at three scanning speeds. In the "slow" mode a complete line scan, i.e., a back-and-forth deflection in the x direction, required 4.55 ms, whereas 2.22 ms or 1.05 ms was required in the "normal" and "fast" modes. In addition, bidirectional scanning could be selected to yield a minimum of 0.525 ms per line scan. By means of the zoom factor, the length of the imaged line could be varied between 3.13 and 100 μm when a 100× objective was used. With a 40× or 16× objective, correspondingly larger lines were imaged. Independently of the length of the imaged line the number of pixels could be chosen to be between 128 and 1024 per line.

LINESCAMP measurements were coordinated by a fast personal computer (Intel Pentium 90, SMC I/O onboard) and dedicated software, the LINESCAMP Program. The program, written in C, was based on principles similar to those described previously for SCAMP measurements (Wedekind et al., 1994). However, because a faster computer and a new CLSM with improved hardware and software were used in the present study, the program was widely modified. The program used two signals provided by the CLSM's trigger interface to perform the tasks indicated in Fig. 1. The input signals were "Scan," which indicated the beginning of a scan, and "Line-Start," which marked the subsequent beginning of the line. Based on this information, the program adjusted the laser power to imaging or bleaching levels. The way this goal was achieved depended on the operational mode of the AOM. The number of imaging lines before photobleaching, the number of bleaching lines, and positions and lengths of photobleached sections on that line could be defined at will. To avoid photobleaching during monitoring, the imaging laser could be completely switched off for selected time intervals during extended monitor measurements.

The LINESCAMP was optimized for high temporal resolution. If desired, however, the temporal resolution could easily be reduced by either of two methods. In the line-averaging mode of the CLSM, a selectable number of line scans (maximum 512) is recorded and averaged before being written into memory. Thus, in the slow line-scanning mode the time per averaged line scan could be extended to a maximum of 2.329 s, corresponding to about 40 min per frame of 1024 lines. The second

possibility was to simply extend the acquisition time by recording a continuous series of line-scanning images. In that case the total monitoring time was only limited by the available computer memory.

RESULTS AND DISCUSSION

Resolution of confocal imaging and radius of the laser beam focus in the LINESCAMP instrument

The resolution of the confocal microscope used in this study was determined for three objective lenses for a detection pinhole diameter of 4 optical units. FITC-labeled beads (Sigma) of 105 nm diameter were imaged in the fluorescence mode by both x, y and x, z scans. From these images axial and radial intensity profiles of individual beads were obtained, averaged, and then fitted by Gaussians. These Gaussians were employed as the respective imaging point spread functions. The e^{-2} radii obtained in this manner for the x and y axes varied between 0.18 and 0.41 μm, and those for the z axis between 0.51 and 4.4 μm, depending on the objective. The complete data are given in Table 1.

The radius of the laser beam in the focal plane of the CLSM was determined by the gold edge method according to Schneider and Webb (1981) and Petersen et al. (1986). In short, the broken edge of a gold-sputtered coverslip was imaged in the reflection mode for various settings of the detection pinhole. Intensity profiles across the broken edge were obtained, differentiated, and fitted by Gaussians. The e^{-2} radii of the best-fitting Gaussians were plotted as a function of the pinhole diameter, and the limiting values were determined by extrapolation to an infinitely large pinhole. The resulting limiting values divided by 2 were used as standard deviations of the illuminating spots (i.e., as σ_{NA} in Eq. 1). The e^{-2} radii for the three objective lenses employed are given in Table 1.

Spatial selectivity and efficiency of photobleaching in the LINESCAMP instrument

The capability of the LINESCAMP instrument to selectively photolyse line segments of predetermined size and number was tested with thin layers of polyacrylamide gels containing immobilized FITC-dextrans. As illustrated in Fig. 3, the LINESCAMP was able to fulfill this task. By gradually reducing the length of the photobleached segment, the diffraction limit was approached. Thus, although the LINESCAMPER could be instructed to switch on the photobleaching laser beam for a single pixel only (of, e.g., 0.02 μm length), the actual size of the photobleached segment was determined by the diffraction-limited diameter of the illuminating laser spot. This was studied experimentally by reducing the length of the photobleached line segment to a minimum (lower line in Fig. 3 *A*) and then imaging the minimum bleached area by both x,y scans (Fig. 3 *A*) and x,z scans (Fig. 3 *B*). The images were evaluated for the intensity profiles of the bleached area in the x, y, and z directions. These profiles were fitted by Gaussians and deconvoluted with regard to the microscope point spread function to account for the limited imaging resolution. In case of the 100×, NA 1.3 oil immersion objective, the e^{-2} distances of the deconvoluted intensity profiles of the smallest photobleached areas were thus found to be 0.27, 0.22, and 1.1 μm for the x, y, and z axes, respectively, in reasonable agreement with expectations based on an e^{-2} radius of the laser beam of 0.17 μm.

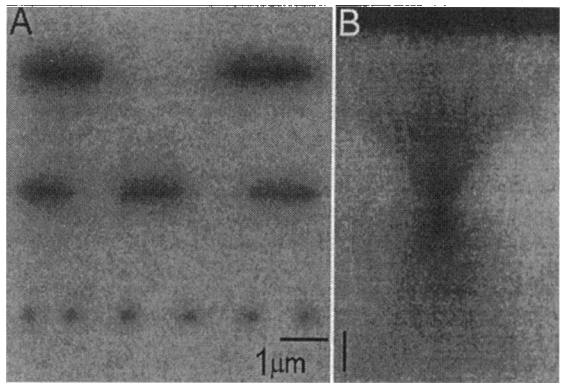

FIGURE 3 Visualization of areas photobleached by line-scanning microphotolysis. Thin gel layers containing immobilized, fluorescently labeled macromolecules were employed to visualize the geometry of photobleaching patterns. (*A*) The SCAMPER was programmed to photolyse (50 scans) line segments of decreasing length down to the diffraction limit (100×, NA 1.3 objective lens). The result was subsequently visualized by an xy scan. (*b*) xz scan of one of the small, diffraction-limited photolysed line segments.

TABLE 1 Characteristics of the instrument for line-scanning microphotolysis with regard to imaging resolution, laser beam radius, and photobleaching efficiency

Objective lens	Imaging resolution* (μm)		Radius of laser beam# (μm)	Photobleaching efficiency§ (residual fluorescence in % of the initial value)	
	x, y	z		After 1 scan	After 10 scans
16× NA 0.5	0.41	4.40	0.47	76	36
40× NA 1.0	0.24	1.17	0.24	83	49
100× NA 1.3	0.18	0.51	0.17	92	52

*e^{-2} radius of the confocal image of FITC-labeled beads with 105-nm diameter.
#e^{-2} radius of the laser beam in the focal plane of the CLSM as determined by the gold-edge method.
§Residual fluorescence of a thin gel layer containing immobile FITC-dextran after one or ten scans as a percentage of the initial fluorescence at a beam power of 1 mW in the object and using the medium scanning speed.

Thin gel layers containing immobilized FITC-dextrans were also used to assess the efficiency of photobleaching. A line segment was repeatedly photobleached, and the fluorescence originating from the photolysed segment was monitored during photobleaching, employing an appropriate small photomultiplier voltage. Thus, the reduction of fluorescence by photobleaching could be directly followed scan by scan. An example of such measurements, employing the 40×, NA 1.0 objective lens; the medium scan speed (2.2 ms per line); a segment of nominally 300 nm length; and a laser beam power of 1 mW in the sample, is shown in Fig. 4. Values for the photobleaching efficiency at other conditions are given in Table 1. The results show that in general a single scan or a few scans were sufficient to substantially reduce the fluorescence of FITC-dextrans.

Lateral diffusion measurements at diffraction-limited spatial resolution

The capabilities of the LINESCAMP method for two-dimensional lateral diffusion measurements at high spatial resolution were tested with simple systems. To cover a wide range of diffusion coefficients, FITC-dextrans of various molecular weights were dissolved in water-glycerine mixtures of different viscosities and spread as very thin layers between a glass slide and a coverslip. An example, for a typical measurement employing the 40×, NA 1.0 objective lens and the medium scanning speed (2.2 ms per line), is shown in Fig. 5. A thin layer of a FITC-dextran of 2000 kDa molecular mass in a glycerine-water mixture (70/30 by weight) was used as a sample. Before the measurement an x,y scan had been obtained to select a line and mark on it several segments for photobleaching. The length of the segments was chosen to be 0.55 μm, to be close to the diffraction limit (cf. Table 1). The LINESCAMP experiment yielded an x,t image (Fig. 5), revealing three time domains: prebleaching, bleaching, and postbleaching. In each of the selected line segments the fluorescence substantially decreased by photobleaching and then recovered with time by lateral diffusion. It is noteworthy that the photobleaching traces were straight parallel lines, an immediate and direct indication of the absence of convective flow.

The analysis of the data of Fig. 5 in terms of the lateral diffusion coefficient and the mobile fraction followed the theoretical framework outlined above and is illustrated in Fig. 6. For each of the photobleached segments the averaged intensity was plotted versus time to yield fluorescence recovery curves. The graphs labeled by *a–f* in Fig. 6 correspond directly to traces *a–f* in Fig. 5. The experimental data

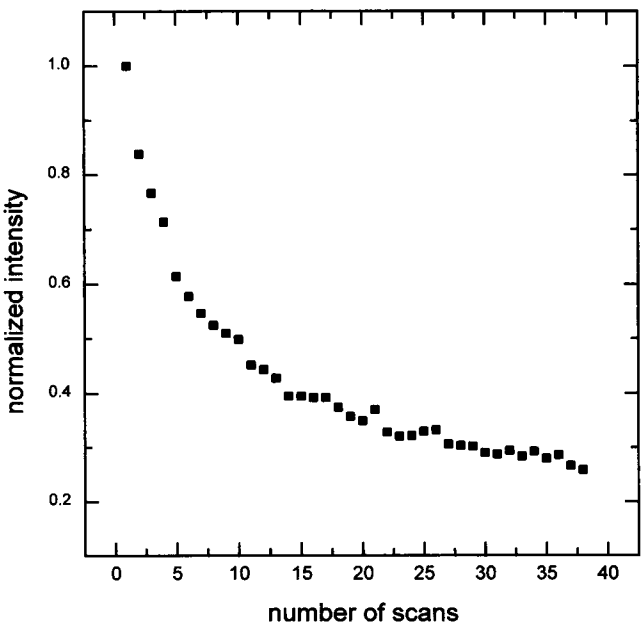

FIGURE 4 Efficiency of photobleaching in line-scanning microphotolysis. In a thin gel layer containing immobilized fluorescently labeled macromolecules a predetermined line segment was repetitively photolysed (analogous to the situation indicated in Fig. 1). During photolysis the fluorescence of the segment was monitored to assess the efficiency of photobleaching. The experiment was performed with a 40×, NA 1.0 objective lens at approximately 1 mW laser power in the object. For other conditions, see Table 1.

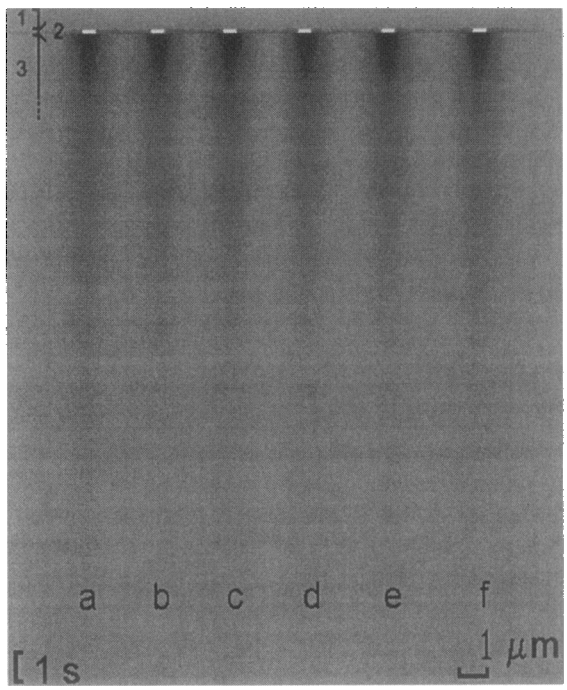

FIGURE 5 Measurement of lateral diffusion by line-scanning microphotolysis using small diffraction-limited photolysed areas. A thin layer of a solution of a FITC-dextran (2000 kDa) in a glycerine-water mixture (70/30 by weight) was used as a test sample. Six segments of 0.55 μm length were chosen along a line for photobleaching. Because the 40× NA 1.0 objective was employed, the laser beam had an e^{-2} radius of 0.24 μm (cf. Table 1), and the photobleached segments thus were diffraction limited. During the bleaching scan the laser power was 1.0 mW in the object. The experiment yielded an "image" with the x position (abscissa) and time (ordinate) as coordinates and with the origin at the left upper corner. The prebleaching, bleaching, and the postbleaching domains are indicated by 1, 2, and 3, respectively.

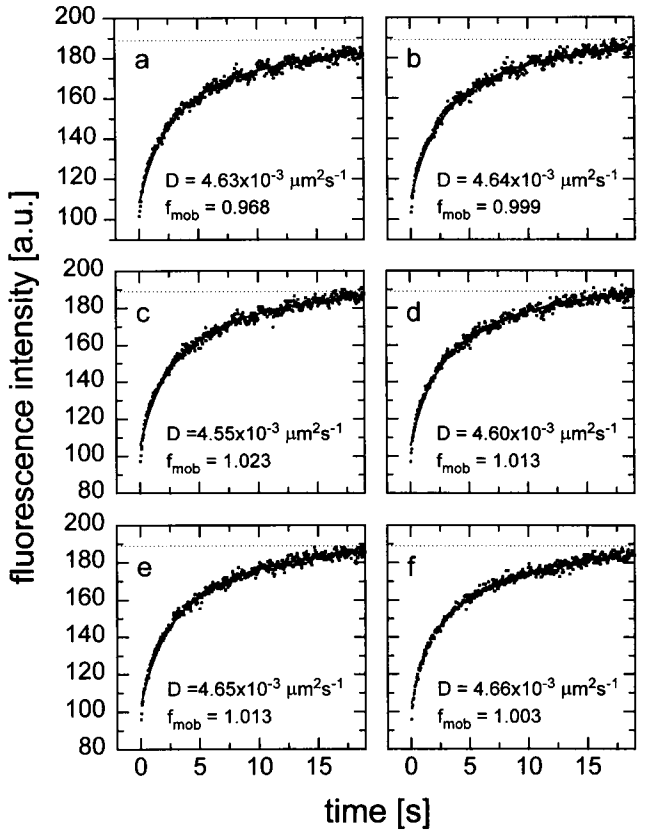

FIGURE 6 Evaluation of lateral diffusion measurements using small diffraction-limited photolysed areas. The experiment shown in Fig. 5 was evaluated by plotting the averaged intensities of the photolysed segments versus time after photolysis. This yielded the fluorescence recovery curves *a–f* (corresponding directly to traces *a–f* of Fig. 5). The experimental data (square symbols) were fitted by Eqs. 1–4 (full lines) to yield the diffusion coefficient D and the mobile fraction f_{mob}, as indicated in the figure.

(squares) were then fitted by Eqs. 1–4 (full lines). The results for the individual photobleached segments are denoted in the figure. On average, D amounted to (4.62 ± 0.04) × 10^{-3} $\mu m^2\ s^{-1}$, and f_{mob} to 1.003 ± 0.020 (mean ± SD), suggesting a favorable reproducibility.

The accuracy and range of LINESCAMP diffusion measurements at diffraction-limited resolution was studied by a direct comparison with lateral diffusion measurements performed on identical samples by the SCAMP method. SCAMP and its application to lateral diffusion measurements has been described in detail (Wedekind et al., 1994; Kubitscheck et al., 1994). In the present case, SCAMP was used to homogeneously photobleach a circular area of 3.7 μm radius. The intensity in the photobleached area, derived from repetitive *x-y* scans, was averaged, plotted versus time, and evaluated for D and f_{mob}, employing the theoretical methods of Axelrod et al. (1976) and Soumpasis (1983). To vary the diffusion coefficients over a broad range, FITC-dextrans were dissolved in glycerine-water mixtures using dextrans of 40–2000 kDa and glycerine/water ratios of 0.4–0.9 (w/w). For each specimen LINESCAMP and SCAMP measurements were performed immediately after each other on the same or closely neighboring sites. The results of these comparative measurements are given in Fig. 7, as far as D is concerned. The mobile fraction was close to unity in all cases and therefore is not shown. Fig. 7 shows a good agreement of LINESCAMP and SCAMP results over the range of diffusion coefficients studied, approximately 10^{-4} to 0.5 $\mu m^2\ s^{-1}$. This suggests that the LINESCAMP method is particularly well suited to the study of lateral mobility at high spatial resolution in viscous systems, e.g., cell membranes.

This conclusion is supported by theoretical considerations. The upper limit for the diffusion coefficient D to be determined by the LINESCAMP method can be roughly estimated from $D \approx r^2/4t_D$, where r is the radius of the bleached area and t_D is the characteristic diffusion time. The smallest possible r is about 0.18 μm (Table 1). The characteristic diffusion time t_D has to be at least 10 times larger than the temporal resolution of the measurements given by the line repetition time of 0.5 ms. With these values the largest diffusion coefficient that can be measured at the highest spatial resolution amounts to ~1.5 $\mu m^2/s$. Larger diffusion coefficients should be accessible at reduced spatial resolution.

To further test for the correctness of LINESCAMP measurements, we measured the lateral diffusion coefficient of b-phycoerythrin in glycerol/water mixtures spread as very thin layers between slides and coverslips. LINESCAMP measurements were performed employing the 40×, NA 1.0 objective and a diffraction-limited photobleached area. In 15 separate series of measurements comprising a total of 150 individual measurements, the lateral diffusion coeffi-

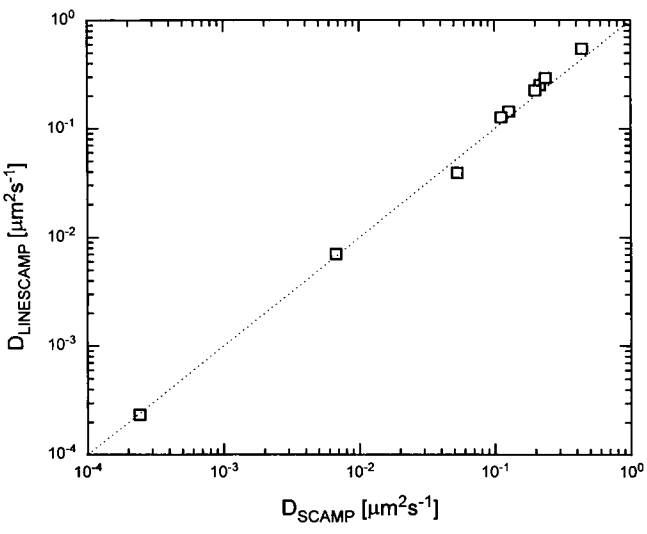

FIGURE 7 Accuracy and range of diffraction-limited diffusion measurements. Diffusion measurements were made on identical samples by both line-scanning microphotolysis and scanning microphotolysis, employing a small diffraction-limited spot in the former and a circular area of 3.6 μm radius in the latter case. The determined standard deviations are smaller than the plotted symbols. Within experimental reproducibility the diffusion coefficients were the same over a range of approximately 10^{-4} to 10^0 $\mu m^2/s$.

cient of b-phycoerythrin was found to be 0.21 ± 0.11 $\mu m^2 s^{-1}$ (mean ± SD) in a glycerol/water mixture of 89.85/11.15 (w/w) at 25°C. To estimate the theoretical lateral diffusion coefficient of b-phycoerythrin according to the Stokes-Einstein equation $D = kT/f$, where k is the Boltzmann constant, T is absolute temperature, and f is the viscous drag coefficient, we approximated the b-phycoerythrin hexamer by a prolate ellipsoid of revolution. For this f is given by $6\pi\eta a/\ln(2a/b)$ (Berg, 1983), where η is solvent viscosity. According to an x-ray analysis at 0.23 nm resolution (Ficner and Huber, 1993), the b-phycoerythrin hexamer has a discoid shape with a diameter of $2a = 11$ nm and a thickness of $2b = 6$ nm. Using, furthermore, a value of 225 cP for η, as extrapolated from the data in the *Handbook of Chemistry and Physics* (Weast and Astle, 1979), the theoretical diffusion coefficient amounted to 0.225 $\mu m^2 s^{-1}$ and thus agreed well with the measured value.

Lateral diffusion measurements at different sizes of the photobleached area

A simple means of changing the size of the photobleached area is to use objective lenses with different NAs. The radius of the laser beam increases (Table 1) from 0.17 to 0.24 μm or to 0.47 μm when exchanging the 100×, NA 1.3 objective for the 40×, NA 1.0 or the 16×, NA 0.5 one. Employing a thin layer of a solution of a FITC-dextran (2000 kDa) in a glycerine-water mixture (40% by weight), LINESCAMP measurements were performed with all three objectives. In each case the size of the photobleached area was diffraction limited. The results are given in Table 2 and show that, within experimental accuracy, the same diffusion coefficients were obtained for all conditions. Moreover, measurements performed by the SCAMP method on the same samples yielded the same diffusion coefficients as obtained by LINESCAMP.

The LINESCAMP method offers a simple method for changing the size and shape of the photobleached area: elongation of the photobleached line segment. A typical example for such measurements is given in Fig. 8. Employing again a thin layer of a solution of a FITC-dextran in a glycerine-water mixture and the 40×, NA 1.0 objective, the length of the photobleached line segment was increased in several steps from the diffraction limit of approximately 0.54 μm to 1.64 μm. The photobleaching recovery curves derived from this experiment are shown in Fig. 9. Upon evaluation of the experimental data (symbols) by Eqs. 1–4, the best fitting curves (full lines) were obtained. The values for the diffusion coefficients are given in Table 3. It can be seen that the same coefficients were obtained within experimental accuracy for the differing line segments.

As mentioned in the theory section, the methods used to evaluate conventional photobleaching experiments for lateral mobility parameters according to Axelrod et al. (1976) and Soumpasis (1983) do not apply to the present case, at least not in a rigorous sense. The conventional analysis pertains to experiments employing a stationary and axially symmetric laser beam, whereas the LINESCAMP method uses a scanned beam and may involve photobleached areas that are either almost axially symmetric or not at all, depending on the length of the line segment photobleached (Fig. 3 *A*). However, at least in the case of the diffraction-limited, almost axially symmetric photobleached area, the differences of the premises on which the conventional analysis or the numerical methods presented here are based are not very large. We found it interesting therefore to apply the conventional analysis to the present data and to compare the results with those of the numerical simulation. This has been

TABLE 2 Lateral diffusion measurements by line-scanning microphotolysis employing a diffraction-limited photobleached area

Objective lens	D ($\mu m^2/s$)*	
	LINESCAMP	SCAMP#
16× NA 0.5	0.200 ± 0.014	0.211 ± 0.019
40× NA 1.0	0.225 ± 0.023	0.218 ± 0.013
100× NA 1.3	0.233 ± 0.016	0.216 ± 0.013

*Lateral diffusion coefficient (mean ± SD of 5–10 measurements) of a FITC-dextran of 2000 kDa molecular mass in a 40% (w/w) glycerine-water mixture.

#In SCAMP measurements a circular area of 3.6 μm diameter was homogeneously photobleached and the fluorescence recovery, derived from repetitive x-y scans, was analyzed according to the method of Axelrod et al. (1976) and Soumpasis (1983), as described previously (Kubitscheck et al., 1994).

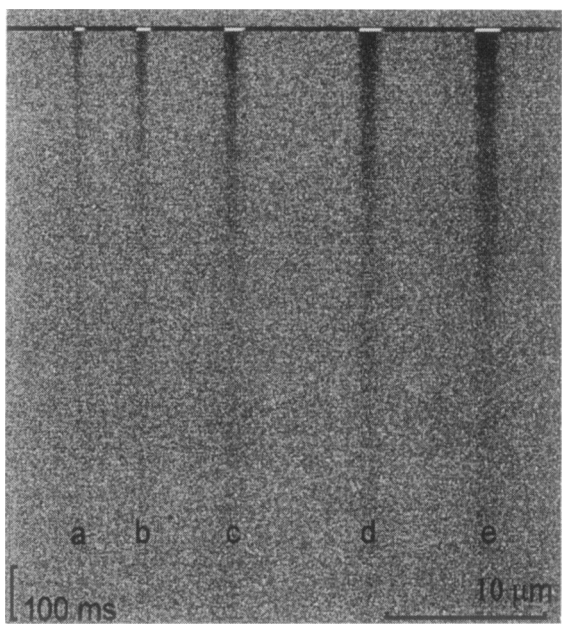

FIGURE 8 Measurement of lateral diffusion by line-scanning microphotolysis employing line segments of increasing lengths. A thin layer of a solution of FITC-dextran (2000 kDa) in a glycerine-water mixture (20/80 by weight) was used as a test sample. Segments of increasing length (0.54, 0.82, 1.23, 1.36, and 1.64 μm) were chosen along a line for photobleaching, and a measurement with a 40×, NA 1.0 objective lens was performed at 1.1 mW laser power in the object.

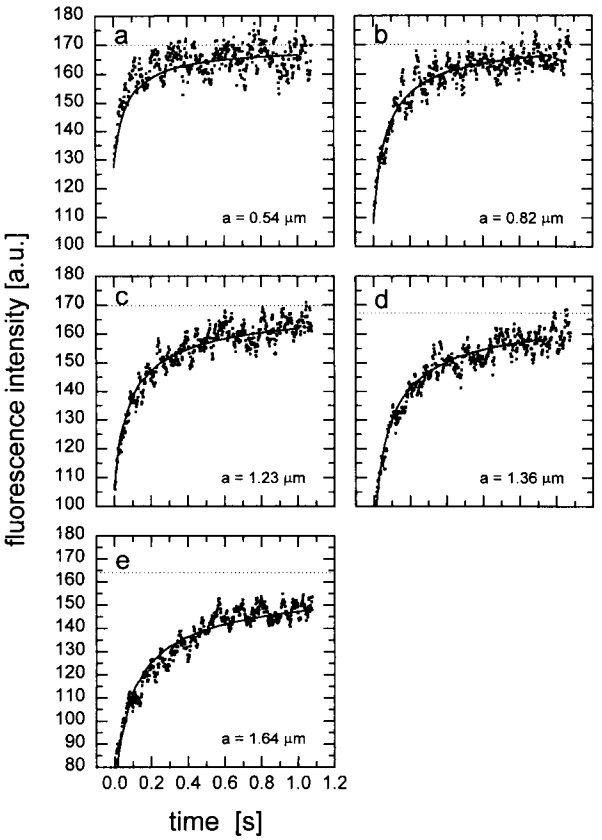

FIGURE 9 Evaluation of lateral diffusion measurements using line segments of different length. The experiment shown in Fig. 8 was evaluated by plotting the intensities of the photolysed segments versus time after photolysis. This yielded the fluorescence recovery curves *a–e* (corresponding directly to traces *a–e* of Fig. 8). The experimental data (square symbols) were fitted by Eqs. 1–4 (full lines) to obtain the diffusion coefficient D and the mobile fraction f_{mob}. The length a of the photobleached segment is indicated. In spite of the different recovery kinetics, the evaluation yielded the same diffusion coefficients for all line segments (cf. Table 3).

done for the data of Fig. 9, and the outcome is listed in Table 3. As the radius of the photobleached area in the conventional analysis, we chose that of a circle having the same area as the actually photobleached one. Table 3 suggests that the conventional analysis yields results similar to those of the numerical simulation in the case of diffraction-limited, almost axially symmetric photobleached areas. However, with increasing length of the photobleached line segment, the differences between conventional analysis and numerical simulation become substantial.

TABLE 3 Analysis of lateral diffusion measurements using differently sized line segments and their evaluation by either numerical simulation or the approach used commonly for conventional photobleaching experiments

	D ($\mu m^2/s$)*	
Length of the photobleached line segment (μm)	Numerical simulation	Analysis according to Axelrod et al. (1976)
a) 0.54	0.48	0.56
b) 0.82	0.46	0.36
c) 1.23	0.42	0.39
d) 1.37	0.47	0.42
e) 1.64	0.42	0.29

*Lateral diffusion coefficient of a FITC-dextran of 2000 kDa molecular mass in a 20% (w/w) glycerine-water mixture.

Preliminary measurements of intranuclear lateral mobility

We are interested in the lateral mobility of macromolecules inside the cell nucleus, as described in the Conclusion. Therefore we have conducted preliminary experiments to find out whether the LINESCAMP method is suitable for this purpose. 3T3 cells were permeabilized with Triton X-100 and incubated with FITC-dextran of 150 kDa molecular mass. The dextran could easily permeate into the cell nuclei, indicating that the nuclear pores, and possibly the nuclear envelope altogether, had been removed. Surprisingly, however, the nuclear interior did not appear homogeneously fluorescent. Instead, an elaborate network of less fluorescent, apparently interconnected fibers, dots, and granules became visible, as shown in Fig. 10. The identity of these structures has not yet been established, but obviously should be related to chromatin. The larger dark areas probably represent nucleoli.

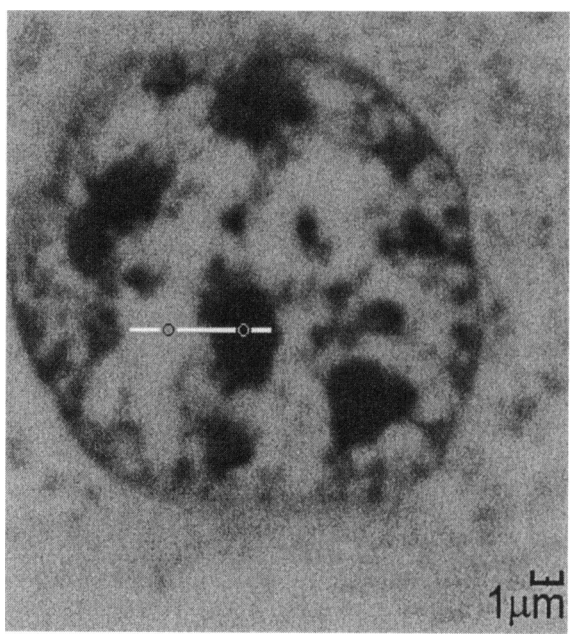

FIGURE 10 Application of line-scanning microphotolysis to lateral diffusion in the cell nucleus. 3T3 cells were permeabilized with Triton X-100 and incubated with a FITC-dextran of 150 kDa. The figure shows a confocal section (*xy* scan) taken through the center of a nucleus at high magnification using the 100×, NA 1.3 objective lens. An elaborate network of less fluorescent, apparently interconnected fibers, dots, and granules is visible. The identity of the structures is not known, but they are probably related to chromatin. The line selected for the lateral diffusion measurement (shown in Fig. 11) is indicated, as well as the location and size (e^{-2} radius) of the two photobleached areas.

Using LINESCAMP, mobility measurements were performed inside single nuclei. An example of such measurements is shown in Fig. 11. The intranuclear sites of these measurements together with the e^{-2} radii of the bleached spots are indicated in Fig. 10. The photobleaching curves (Fig. 11 *A*) suggest that distinct differences exist, even after normalization (Fig. 11 *B*). A further evaluation of the data was not attempted at present because diffusion in the cell nucleus is clearly a three-dimensional process not covered by the theory presented in the present paper (cf. the Conclusion). Nevertheless, the measurements demonstrate that the LINESCAMP method can be applied to spatially resolved mobility measurements in the cell nucleus and is able to pick up local mobility differences.

CONCLUSION

The paper describes a new method for the study of molecular transport in microscopic systems. Referred to as LINESCAMP, the method combines microphotolysis with confocal scanning and is characterized by a maximum temporal resolution of ~0.5 ms and a maximum lateral resolution of ~0.34 μm. In effect, the new method is a high-resolution version of the SCAMP method that was described recently (Wedekind et al., 1994). SCAMP also features a high spatial but a much smaller temporal (~100 ms) resolution. In principle, the increase in temporal resolution was made possible by employing the line scan mode of the CLSM. A number of additional technical improvements were necessary to put the concept into practice. Thus, the AOM of the SCAMPER was operated in the analog mode, permitting us to switch the laser beam power between monitoring and photolysing levels in less then a microsecond. A more accurate control of beam switching was obtained by using a faster computer and improved programming. Furthermore, the availability of a confocal microscope of latest design, featuring an improved transmission of the laser beam as well as a better utilization of the fluorescence emitted by the sample, was essential.

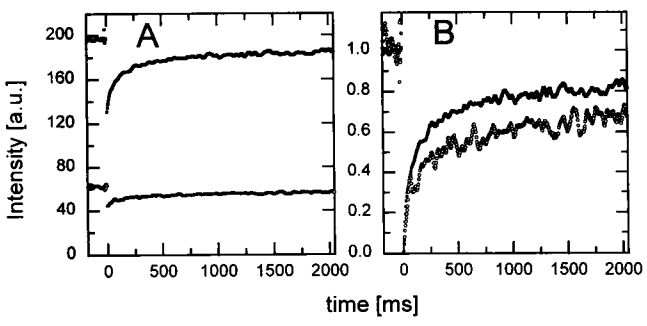

FIGURE 11 Mobility of a 150-kDa FITC-dextran in the nucleus. The fluorescence recovery curves obtained in the experiment outlined in Fig. 10 are given (*a*) before and (*b*) after normalization to the fluorescence before photobleaching. The upper curves refer to the left spot of Fig. 10, and the lower curves refer to the right spot.

Together with the instrumentation, a theoretical framework for the evaluation of diffusion measurements was developed. Based on the numerical simulation of diffusion processes using a modified two-dimensional Crank-Nicholson iteration scheme, the approach has the advantage that it can be applied to any arbitrary initial condition, and not just to photobleached areas of axial symmetry. Moreover, the extension of the theory to three-dimensional diffusion is conceptually and computationally straightforward. The theory could also easily be extended to rather complicated processes, such as those encountered in continuous microphotolysis (Peters et al., 1981), in which photobleaching and lateral diffusion proceed simultaneously.

The possibility of extending the current experimental and theoretical methods to three-dimensional molecular transport appears particularly important to us. As mentioned in the Introduction, the cell nucleus is thought to comprise an intricate system of chromosome domains and interchromatin channels (Manuelidis, 1985; Schardin et al., 1985; Pinkel et al., 1988; De Boni, 1994; Blobel, 1985; Spector, 1990; Cremer et al., 1993; Zachar et al., 1993). It may well be that this three-dimensional arrangement of chromosomes ultimately encodes the three-dimensional arrangement of cellular components, and as a consequence the three-dimensional building plan of the organism. In this scenario the interchromatin channels assume a crucial role because they may selectively direct certain transcription products from specific genes to specific sites of the nuclear periphery. Therefore, the experimental characterization of intranuclear transport could shed light on the intranuclear organization and help to test the outlined hypothesis.

So far, we have observed that the LINESCAMP method can be used in principle to perform spatially resolved measurements of lateral transport in cell nuclei. In these measurements the resolution in the x,y plane was quite good (~0.34 μm) but much poorer (~1.1 μm) in the z direction. This, however, might be improved by application of two-photon excitation (Denk et al., 1990), which yields a true confinement of the excitation volume, also in the z direction. We have shown (Kubitscheck et al., 1996) that two-photon absorption can be combined with the SCAMP method to permit spatially resolved transport measurements in three-dimensional cellular arrays. The combination of the LINESCAMP method with two-photon absorption, and the extension of the theoretical description from two- to three-dimensional problems, has yet to be achieved, but this is currently being worked on in our laboratory.

APPENDIX: NUMERICAL SOLUTION OF THE DIFFUSION EQUATION FOR ARBITRARY INITIAL CONDITIONS

For one-dimensional diffusion the Crank-Nicholson scheme is given by (Crank, 1975)

$$\frac{C_l^{n+1} - C_l^n}{\Delta t} = \frac{D}{2}\left[\frac{(C_{l-1}^{n+1} - 2C_l^{n+1} + C_{l+1}^{n+1}) + (C_{l-1}^n - 2C_l^n + C_{l+1}^n)}{\Delta x^2}\right]. \quad \text{(A1)}$$

Here the indices n and l describe the time and space discretization, respectively. Setting $D\Delta t/\Delta x^2 \equiv 1$, this results in a tridiagonal matrix system for C_l^{n+1}:

$$-C_{l-1}^{n+1} + 4C_l^{n+1} - C_{l+1}^{n+1} = C_{l-1}^n + C_{l+1}^n, \quad \text{(A2)}$$

$$-C_{j-1,l}^{n+1} - C_{j,l-1}^{n+1} + 6C_{j,l}^{n+1} - C_{j+1,l}^{n+1} - C_{j,l+1}^{n+1} = 2C_{j,l}^n + C_{j-1,l}^n + C_{j+1,l}^n + C_{j,l-1}^n + C_{j,l+1}^n, \quad \text{(A3)}$$

that can easily be solved by standard techniques (Crank, 1975; Press et al., 1992). In a system with two space dimensions, and $D\Delta t/\Delta x^2 = D\Delta t/\Delta y^2 \equiv 1$, the corresponding discretization reads

$$-C_{j-1,l}^{n+1/2} + 4C_{j,l}^{n+1/2} - C_{j+1,l}^{n+1/2} = C_{j,l-1}^n + C_{j,l+1}^n \quad \text{(A4a)}$$

where the indices l, j, and n denote the discretization in x, y, and time coordinates, respectively. The evolving matrices are no longer tridiagonal and hence require significantly more computation time to be solved. Therefore, we applied the alternating-direction implicit method using the concept of time step splitting (Ames, 1977; Press et al., 1992). The principal idea was to divide each time step into two substeps of $\Delta t/2$. In each substep, a different dimension was treated implicitly. This led to the following discretization scheme:

$$-C_{j,l-1}^{n+1} + 4C_{j,l}^{n+1} - C_{j,l+1}^{n+1} = C_{j-1,l}^{n+1/2} + C_{j+1,l}^{n+1/2}. \quad \text{(A4b)}$$

Using Eq. A4, it was straightforward to calculate $c(x,y,t)$, starting with an arbitrary initial condition under the given boundary conditions.

Support by the Deutsche Forschungsgemeinschaft (grant Pe 138/15-3) is gratefully acknowledged.

REFERENCES

Ames, W. F. 1977. Numerical Methods for Partial Differential Equations, 2nd Ed. Academic Press, New York.

Anderson, C. M., G. N. Georgiou, I. E. G. Morrison, G. V. Stevenson, and R. J. Cherry. 1992. Tracking of cell surface receptors by fluorescence digital imaging microscopy using charge-coupled device camera. Low density lipoprotein and influenza virus receptor mobility at 4°C. *J. Cell Sci.* 101:415–425.

Axelrod, D., D. E. Koppel, J. Schlessinger, E. Elson, and W. W. Webb. 1976. Mobility measurement by analysis of fluorescence photobleaching recovery kinetics. *Biophys. J.* 16:1055–1069.

Barak, L. S., and W. W. Webb. 1981. Fluorescent low density lipoprotein for observation of dynamics of individual receptor complexes on cultured human fibroblasts. *J. Cell Biol.* 90:595–604.

Berg, H. C. 1983. Random Walks in Biology. Princeton University Press, Princeton, NJ.

Berland, K. M., P. T. C. So, and E. Gratton. 1995. Two-photon fluorescence correlation spectroscopy: method and application to the intracellular environment. *Biophys. J.* 68:694–701.

Betzig, E., J. K. Trautman, T. D. Harris, J. S. Weiner, and R. L. Kostelak. 1991. Breaking the diffaction barrier: optical microscopy at a nanometric scale. *Science.* 251:1468–1470.

Blobel, G. 1985. Gene gating: a hypothesis. *Proc. Natl. Acad. Sci. USA.* 82:8527–8529.

Blonk, J. C. G., A. Don, H. van Aalst, and J. J. Birmingham. 1993. Fluorescence photobleaching recovery in the confocal scanning light microscope. *J. Microsc.* 169:363–374.

Born, M., and E. Wolf. 1986. Principles of Optics, 6th Ed. Pergamon, New York.

Crank, J. 1975. The Mathematics of Diffusion, 2nd ed. Oxford University Press, Oxford, UK.

Cremer, T., A. Kurz, R. Zirbel, S. Dietzel, B. Rinke, E. Schrock, M. R. Speicher, U. Mathieu, A. Jauch, P. Emmerich, H. Scherthan, T. Ried, C. Cremer, and P. Lichter. 1993. Role of chromosome territories in the functional compartmentalisation of the cell nucleus. *Cold Spring Harb. Sym. Quant. Biol.* 58:777–792.

De Boni, U. 1994. The interphase nucleus as a dynamic structure. *Int. Rev. Cytol.* 150:149–171.

De Brabander, M., G. Geuens, R. Nuydens, M. Moeremans, and J. de Mey. 1985. Probing microtubule-dependent intracellular mobility with nanometre particle video ultramicroscopy (nanovid ultramicroscopy). *Cytobios.* 43:273–283.

Denk, W., J. H. Strickler, and W. W. Webb. 1990. Two-photon laser scanning microscopy. *Science.* 248:445–458.

Edidin, M. 1992a. Patches, posts and fences: proteins and plasma membrane domains. *Trends Cell Biol.* 2:376–380.

Edidin, M. 1992b. Translational diffusion of membrane proteins. *In* The Structure of Biological Membranes. P. Yeagle, editor. CRC Press, Boca Raton, FL. 539–572.

Edidin, M. 1994. Truncation mutants define and locate cytoplasmic barriers to lateral mobility of membrane glycoproteins. *Proc. Natl. Acad. Sci. USA.* 91:3378–3382.

Edidin, M., Y. Zagyansky, and T. J. Lardner. 1976. Measurement of membrane protein lateral diffusion in single cells. *Science.* 191: 466–468.

Elson, E. L., and D. Magde. 1974. Fluorescence correlation spectroscopy. II. Conceptual basis and theory. *Biopolymers.* 13:1–27.

Ficner, R., and R. Huber. 1993. Refined crystal structure of phycoerythrin from *Porphyridium cruentum* at 0.23-nm resolution and localization of the γ subunit. *Eur. J. Biochem.* 218:103–106.

Ishihara, A., and K. Jacobson. 1993. A closer look at how membrane proteins move. *Biophys. J.* 65:1754–1755.

Jacobson, K., Z. Derzko, E. S. Wu, Y. Hou, and G. Poste. 1976. Measurement of the lateral mobility of cell surface components in single, living cells by fluorescence recovery after photobleaching. *J. Supramol. Struct.* 5:565–576.

Koppel, D. E. 1979. Fluorescence redistribution after photobleaching. A new multipoint analysis of membrane translational dynamics. *Biophys. J.* 28:281–292.

Kubitscheck, U., M. Tschödrich-Rotter, P. Wedekind, and R. Peters. 1996. Two-photon scanning microphotolysis for three-dimensional data storage and biological transport measurements. *J. Microsc.* In press.

Kubitscheck, U., P. Wedekind, and R. Peters. 1994. Lateral diffusion measurements at high spatial resolution by scanning microphotolysis in a confocal microscope. *Biophys. J.* 67:948–956.

Kusumi, A., Y. Sako, and M. Yamamoto. 1993. Confined lateral diffusion of membrane receptors as studied by single particle tracking (nanovid microscopy). Effects of calcium-induced differentiation in cultured epithelial cells. *Biophys. J.* 65:2021–2040.

Lang, I., M. Scholz, and R. Peters. 1986. Molecular mobility and nucleocytoplasmic flux in hepatoma cells. *J. Cell Biol.* 102:1183–1190.

Lewis, A., M. Isaacson, A. Harootunian, and A. Muray. 1984. Development of a 500 Å resolution light microscope. *Ultramicroscopy.* 13: 227–232.

Luby-Phelps, K. 1994. Physical properties of cytoplasm. *Curr. Opin. Cell Biol.* 6:3–9.

Magde, D., E. L. Elson, and W. W. Webb. 1974. Fluorescence correlation spectroscopy. II. An experimental realization. *Biopolymers.* 13:29–61.

Manuelidis, L. 1985. Individual interphase chromosome domains revealed by in situ hybridisation. *Hum. Genet.* 71:288–293.

Peters, R. 1981. Translational diffusion in the plasma membrane of single cells as studied by fluorescence microphotolysis. *Cell. Biol. Int. Rep.* 5:733–760.

Peters, R., A. Brünger, and K. Schulten. 1981. Continuous fluorescence microphotolysis: a sensitive method for study of diffusion processes in single cells. *Proc. Natl. Acad. Sci. USA.* 78:962–966.

Peters, R., J. Peters, K. H. Tews, and W. Bähr. 1974. A microfluorimetric study of translational diffusion in erythrocyte membranes. *Biochim. Biophys. Acta.* 367:282–294.

Peters, R., and M. Scholz. 1991. Fluorescence photobleaching techniques. *In* New Techniques of Optical Microscopy and Microspectroscopy. R. J. Cherry, editor. Macmillan, New York. 199–228.

Petersen, N. O., S. Felder, and E. L. Elson. 1986. Measurement of lateral diffusion by fluorescence photobleaching recovery. *In* Immunochemistry, Vol. 1, 4th Ed. Blackwell Scientific Publications, Oxford.

Pinkel, D., J. Landegent, C. Collins, J. Fuscoe, R. Segraves, J. Lucas, and J. W. Gray. 1988. Fluorescence in situ hybridisation with human chromosome specific libraries: detection of trisomy 21 and translocations of chromosome 4. *Proc. Natl. Acad. Sci. USA.* 85:9138–9142.

Pohl, D. W., W. Denk, and M. Lanz. 1984. Optical stethoscopy: image recording with resolution $\lambda/20$. *Appl. Phys. Lett.* 44:651–653.

Press, W., S. A. Teukolsky, W. V. Vetterling, and B. P. Flannery. 1992. Numerical Recipes in C. Cambridge University Press, Cambridge.

Schardin, M., T. Cremer, H. D. Hager, and M. Lang. 1985. Specific staining of human chromosome position in human chromosome in Chinese hamster × man hybrid cell lines demonstrates interphase chromosome territorries. *Hum. Genet.* 71:281–287.

Schneider, A. M., and W. W. Webb. 1981. Measurement of submicron laser beam radii. *Appl. Optics.* 20:1382–1388.

Schmidt, M., M. Tschödrich-Rotter, R. Peters, and G. Krohne. 1994. Properties of fluorescent labelled Xenopus lamin A in vivo. *Eur. J. Cell Biol.* 65:70–81.

Scholz, M., H. Sauer, H. P. Rihs, and R. Peters. 1988. Laser scanning microscopy to study molecular transport in single cells. *Int. Soc. Opt. Eng. Proc.* 1028:160–166.

Soumpasis, D. M. 1983. Theoretical analysis of fluorescence photobleaching recovery experiments. *Biophys. J.* 41:95–97.

Spector, D. L. 1990. Higher order nuclear organisation: three-dimensional distribution of small nuclear ribonucleoprotein particles. *Proc. Natl. Acad. Sci. USA.* 87:147–151.

Tschödrich-Rotter, M., G. Ogochukwo, U. Kubitscheck, T. Buckley, and R. Peters. 1996. Optical single channel analysis of the aerolysin pore in erythrocyte membranes. *Biophys. J.* 70:723–732.

Weast, R. C., and M. J. Astle, editors. 1979. CRC Handbook of Physics and Chemistry, 60th Ed. CRC Press, Boca Raton, FL. F-62, D-239.

Wedekind, P., U. Kubitscheck, and R. Peters. 1994. Scanning microphotolysis: a new photobleaching technique based on fast intensity modulation of a scanned laser beam and confocal imaging. *J. Microsc.* 176:23–33.

Zachar, Z., J. Kramer, I. P. Mims, and P. M. Bingham. 1993. Evidence of channelled diffusion of pre-mRNAs during nuclear RNA transport in metazoans. *J. Cell. Biol.* 121:729–742.